LAWRENCE
LIVERMORE
NATIONAL
LABORATORY

LLNL-CONF-821609

The role of chemical mechanism in simulations of high-pressure n-dodecane spray pyrolysis

N. J. Killingsworth, T. M. Nguyen, C. Brown, G. Kukkadapu, J. Manin

April 15, 2021

12th U. S. National Combustion Meeting
College Station, TX, United States
May 24, 2021 through May 26, 2021

Disclaimer

Sub Topic: Reacting Kinetics

12th U. S. National Combustion Meeting
Organized by the Central States Section of the Combustion Institute
May 24–26, 2021 (Virtual)
College Station, Texas

The role of chemical mechanism in simulations of high-pressure n-dodecane spray pyrolysis

*Nick J. Killingsworth[1, *], Tuan M. Nguyen[2], Carter Brown[3], Goutham Kukkadapu[1], Julien Manin[2]*

[1]*Lawrence Livermore National Laboratory, Livermore CA, USA*
[2] *Sandia National Laboratories, Livermore CA, USA*
[3] *Department of Mechanical and Aerospace Engineering, University of California, Davis CA, USA*
[*]*Corresponding Author Email: killingsworth2@llnl.gov*

Abstract: We performed Computational Fluid Dynamics (CFD) simulations using a Reynolds-Averaged Navier-Stokes (RANS) turbulence model of high-pressure spray pyrolysis with a detailed chemical kinetic mechanism encompassing pyrolysis of n-dodecane and formation of polycyclic aromatic hydrocarbons. We compare the results using the detailed mechanism and those found using several different reduced chemical mechanisms to experiments carried out in an optically accessible, high-pressure, constant-volume combustion chamber. Three different soot models implemented in the CONVERGE CFD software are used: an empirical soot model, a method of moments, and a discrete sectional method. There is a large variation in the prediction of the soot between different combinations of chemical mechanisms and soot model. Furthermore, the amount of soot produced from all models is substantially less than experimental measurements. All of this indicates that there is still substantial work that needs to be done to arrive at simulations that can be relied on to accurately predict soot formation.
Keywords: Soot, pyrolysis, spray, CFD, chemical kinetics

1. Introduction [12pt]

The emissions from power generation and transportation are major contributors to climate change and the production of particulate matter has a detrimental effect on human health. While there is a strong drive to reduce the number of combustion engines in use, they will remain the principal mode of transportation and power generation for many decades [1], and understanding the processes that govern the formation of particulate matter is likely to lead to many benefits.

Soot formation is a complex phenomenon that does not readily lend itself to experimental observation due to the short time scales of intermediate species and the small size of initial soot particles and their precursors. Computational Fluid Dynamics (CFD) simulations can capture these length and time scales, while also providing a means of understanding the time-history of short lived and intermediate species. However, most chemical kinetic mechanisms are developed to capture global metrics such as the ignition delay and the flame speed. Accurately capturing global metrics and the formation and destruction of the large polycyclic aromatic hydrocarbon (PAH) species that play a key role in soot formation is difficult and requires larger mechanisms which can be computationally prohibitive. Furthermore, soot model development has focused on simple

LLNL-CONF-821609, SAND2021-4734 C

fuels such as ethylene under atmospheric conditions [2]. These modeling efforts also target turbulent reacting flow, where the turbulent flow field and competing effects between the soot inception and oxidation processes can render systematic model examination a challenging task.

In this work, we perform CFD simulations of n-dodecane soot formation process under engine relevant conditions using the CONVERGE commercial software [3]. Examining the soot formation process under oxygen-starved pyrolysis conditions alleviates the difficulties associated with the competing effects between soot growth and oxidation. As a result of the short injection of a small amount of fuel into a comparably large constant-volume chamber, spray vaporization and mixing effects on the soot formation process are minimized. These advantages enable systematic evaluation of different sub-processes associated with modeling soot. Different industry-relevant soot models are examined. Validation against time-resolved soot measurements is also performed. A novel reaction mechanism developed by Lawrence Livermore National Laboratory (LLNL), which provides a detailed description of the formation of PAHs, is compared against various existing chemical mechanisms in the literature.

2. Methods / Experimental

Experiments

Soot formation was compared to the experimental results of Skeen and Yasutomi [4]. N-dodecane fuel sprays are injected into an optically accessible, high-pressure, constant-volume combustion chamber capable of emulating ambient conditions up to 1800 K and 350 atm. The experiments were performed using a 0.186-mm diameter single-hole research nozzle. The objective of the injection system and its operation was to produce small quantities of fuel injected over a relatively short period to decouple injection, evaporation and mixing to soot formation, as much as possible.

Soot volume fraction measurements were carried out via diffuse back-illumination extinction imaging (DBI-EI). The reader is referred to Ref. [4] for details of the experimental setup and procedures to extract soot concentration levels. There are many sources of experimental uncertainties such as the soot mass density, the soot non-dimensional extinction coefficient, or the injected fuel mass. The first two sources have been the subject of countless publications and will not be discussed here. On the other hand, the uncertainty associated with the injected fuel quantity is a crucial boundary condition to the current CFD study and will be described in detail in the *CFD Boundary Conditions* section.

Computational Setup

Simulations of the experimental configuration are performed using the commercial CFD code CONVERGE v3.0 [3]. Turbulence is modeled using a standard k-ε Reynolds-averaged Navier–Stokes (RANS) [5] model. A base 4 mm grid size is used throughout the domain. A conical fixed embedding region with a refining scale of 5 is applied between the injector outlet to 7 mm downstream. The same refining scale is used for Adaptive Mesh Refinement (AMR) in the regions where either the sub-grid velocity or temperature exceeds 0.1% or 2.5 % of the respective variable characteristic scale in the domain. The finest resolution of the simulation is thus 62.5 μm. The peak cell count is around 5 million cells for most simulations. Unity Lewis number is assumed.

Liquid spray is modeled using Lagrangian parcel method. Droplet breakup is modelled using the Kelvin-Helmholtz (KH) and Rayleigh-Taylor (RT) [6] [7]. Droplet collisions are modelled using

the no time counter (NTC) algorithm [8]. Droplet drag and evaporation are modeled using the Corrected Distortion framework [9].

Combustion is modeled using a well-mixed reactor model with a multi-zone scheme to group similar computational cells together based on the temperature and mass fraction of two species. The chemistry solver is therefore called once per group rather than for each individual cell, which greatly improves computational efficiency [10]. Temperature is grouped in 5-K bins, and mass fractions in 0.001 bin-width for n-dodecane ($C_{12}H_{26}$) and acetylene (C_2H_2). Acetylene was chosen for its importance in the soot formation process [11], while providing a good way to segregate cells into bins that differ in their chemical reactivity under pyrolysis conditions. The largest chemical mechanism used here consists of more than 800 species, which results in a sparse Jacobian matrix. Therefore, the preconditioned iterative SAGE kinetics solver is used [3].

CFD Boundary conditions

As mentioned earlier, the analysis carried out by Skeen and Yasutomi [4] revealed uncertainties in the injected fuel mass. Because no experimental data were available to extract accurate rate of injection information under these conditions, internal flow CFD simulations were performed using the authors' understanding of the start and end of needle injection dynamics [13], [14]. The internal flow simulation results provide the necessary guidance to construct different rate of injection profiles. These profiles, together with ambient density and temperature, fuel density, orifice diameter, hydraulic coefficients, and spreading angle are then used as inputs to the Musculus and Kattke jet model [15]. This model has demonstrated good agreements when compared to advanced measurements combining high-sensitivity schlieren imaging and planar laser Rayleigh scattering [16]. The modeled penetration rate was then compared to the measurements, and the rate of injection iteratively adjusted until the best match was obtained. The relevant boundary conditions are listed in Table 1.

Table 1: Simulation setup and boundary conditions.

Ambient conditions	
Ambient composition	89.7 % N_2, 6.5 % H_2O, 3.8 % CO_2
Ambient pressure [MPa]	76
Ambient temperature [K]	1500
Ambient density [kg/m^3]	17.6
Injection parameters	
Injector orifice diameter [mm]	0.186
Fuel temperature [°C]	90
Fuel density [kg/m^3]	700
Jet spreading angle [°]	22.0
Discharge coefficient Cd	0.70
Area coefficient Ca	0.98
Injection duration [µs]	140
Injected mass [mg]	0.455

As noted in Table 1, the simulations focus on an ambient temperature of 1500K which is slightly above the 1450-K soot onset temperature measured in the experiments. The ambient pressure of 76 bar aims at being representative of a pressure condition typical of modern boosted diesel engines for light and medium duty applications. The gas composition for the simulations assumes complete reaction of the reactants during the pre-combustion event of the experiments.

Chemical mechanisms

In this section we describe the various n-dodecane chemical kinetic mechanisms used for pyrolysis simulations in this study. Simulations were conducted with three mechanisms from the literature, including the mechanisms of Wang et al. [17] and Narayanaswamy et al. [18], which are popularly used in the literature for spray simulations, and the recent LLNL mechanism of Kukkadapu et al. [19]. The mechanisms of Wang et al. and Narayanaswamy et al. are reduced mechanisms and include both the low temperature oxidation and PAH chemistry. Pyrene isomers (A_4) are the largest PAH's modelled in the mechanism of Wang et al., while the mechanism of Narayanaswamy et al. also describes the formation of cyclopenta-pyrene (A_4R5).

The recent mechanism of Kukkadapu et al. [19] is *a* detailed high temperature mechanism of n-C_{12} and includes PAH chemistry. The original mechanism built in a modular fashion was developed to capture the pyrolysis chemistry of C_1-C_{12} n-alkane, iso-alkane, olefinic, alkynes, and aromatic hydrocarbons, and consist about 1500 species. As the objective of the present study was to study the pyrolysis of n-C_{12}, the mechanism was manually reduced by removing the modules deemed unnecessary (eg: iso-dodecane, iso-octane, iso-nonane, trimethylbenzene etc). Furthermore, the mechanism of Kukkadapu et al. [19] modelled formation of PAH's larger than A_4R5 such as bi-naphthalene isomers, chrysene, *and* triphenylene. During the simulations we noticed that some of the soot models (eg: Gokul model) available in CONVERGE have been developed assuming pyrene is the nucleating species, and the soot contribution from the PAH's larger than pyrene are not always modelled accurately. To get around this problem, the approach of species lumping, the description of reactions leading to formation of larger PAH's were modified with resulting in formation of A_4R5/ *p*yrene, *h*ydrogen molecules as products. A quick summary of the mechanisms and nucleating species used in the simulations is shown in *Table 2*.

Table 2: Chemical mechanisms from the literature used in simulations.

Authors/Reference	# Species	# Reactions	Soot Precursors Used
Wang et al., 2014 [17]	100	432	A_4
Narayanaswamy et al., 2014 [18]	255	1509	A_3R5, A_4, fluoranthene, and A_4R5
Kukkadapu et al., 2020 [19]	872	5611	A_4R5

Soot models

Three different models, representative of the range of soot modeling approaches used in thermal engines, are tested in this work. The first model, developed by Vishwanathan and Reitz [19], describes the overall soot behavior by simulating basic soot processes such as particle inception, surface growth, oxidation, and coagulation. The model provides basic information such as the overall soot mass and number density. The second model, called the Particulate Mimic (PM), is a method of moments approach [20] and provides additional information such as the mean number density and soot volume fraction. The most advanced soot model used in this study, the Particulate Size Mimic (PSM), is based on the discrete sectional method [21], [22]. This model provides more detail about the soot particle distribution function not available from the method of moments. The phenomenological soot model (called Gokul in CONVERGE), has a one-way coupling with the gas phase chemistry such that PAH species that form soot particles are not removed from the gaseous flow field. Consequently, heat and mass transfers are not strictly conserved in this model. In contrast, soot related heat and mass transfer are conserved in both the PM and PSM models.

Table 3: Soot models used in this study.

Model	Soot precursor	Coupling	Details	References
Gokul	Pyrene (A_4)	1-way	Phenomenological	[19]
Particulate Mimic	A_4R5 and/or A_4	2-way	Method of Moments	[20]
Particulate Size Mimic	A_4R5 and/or A_3R5, A_4, fluoranthene	2-way	Sectional Method	[21] [22]

3. Results and Discussion

Simulations with various combinations of the chemical kinetic mechanisms and soot models discussed in the previous section were carried out in CONVERGE at the conditions listed in Table 1. Figure 1 shows the 3-D projected soot mass [kg-m] predicted using the PSM soot model at different time instances for all three chemical mechanisms. These images are obtained by integrating the raw 3-D Eulerian soot mass field in the transverse direction. They qualitatively capture the soot behavior observed from the experimental DBI-EI results (Figure 3 of ref. [4]). The results show that the overall location of soot formation is similar amongst the different simulations, with the Wang et al. mechanism consistently predicting the highest soot mass for all time instances. All three mechanisms also present consistency regarding the temporal evolution of soot formation, with the first time step showing soot being 2 ms ASOI. The soot concentration levels predicted by the Narayanaswamy et al. and Kukkadapu et al. mechanisms are similar. The Kukkadapu et al. mechanism predicts slightly less soot at 2 ms ASOI, but it predicts higher soot concentration at 5 ms ASOI, with higher concentration pockets around 50 mm downstream and away from the jet axis compared to the Narayanaswamy et al. simulations.

We will now explore the effect of the three different soot models listed in Table 3 using the Wang et al. mechanism. The overall soot mass is also compared to the experimental results of Ref. [4]. All soot models use isomers of pyrene, A_4 as the soot precursor. Figure 2a shows profiles of the mass of pyrene normalized by the mass of fuel injected for all three simulations. Because of the one-way coupling in the Gokul model, meaning that mass conservation of combined PAHs and soot is not strictly enforced, pyrene concentration continuously increases. Consequently, this model predicts over two orders of magnitude more pyrene compared to the two-way coupled models. The soot mass predicted by the Gokul model grows exponentially, violating mass conservation. For simulations that include oxidation, this growth is balanced by soot oxidation, resulting in better agreement with engine measurements despite not being physically accurate [19].

By contrast, the PM and PSM models predict just over 15% of the injected fuel is converted to soot, which is significantly lower than the 40% value measured in the experiments and well outside of the expected experimental uncertainty [4]. Beyond the lower conversion efficiency from fuel to soot, or soot yield, the simulations predict a longer soot onset time compared to the experimentally measured soot formation. These large differences highlight the shortcomings of the current models. One contributor is that most kinetic mechanisms are tuned to capture PAH formation under oxidizing engine conditions [16], which can negatively affect their performance under pure pyrolysis conditions.

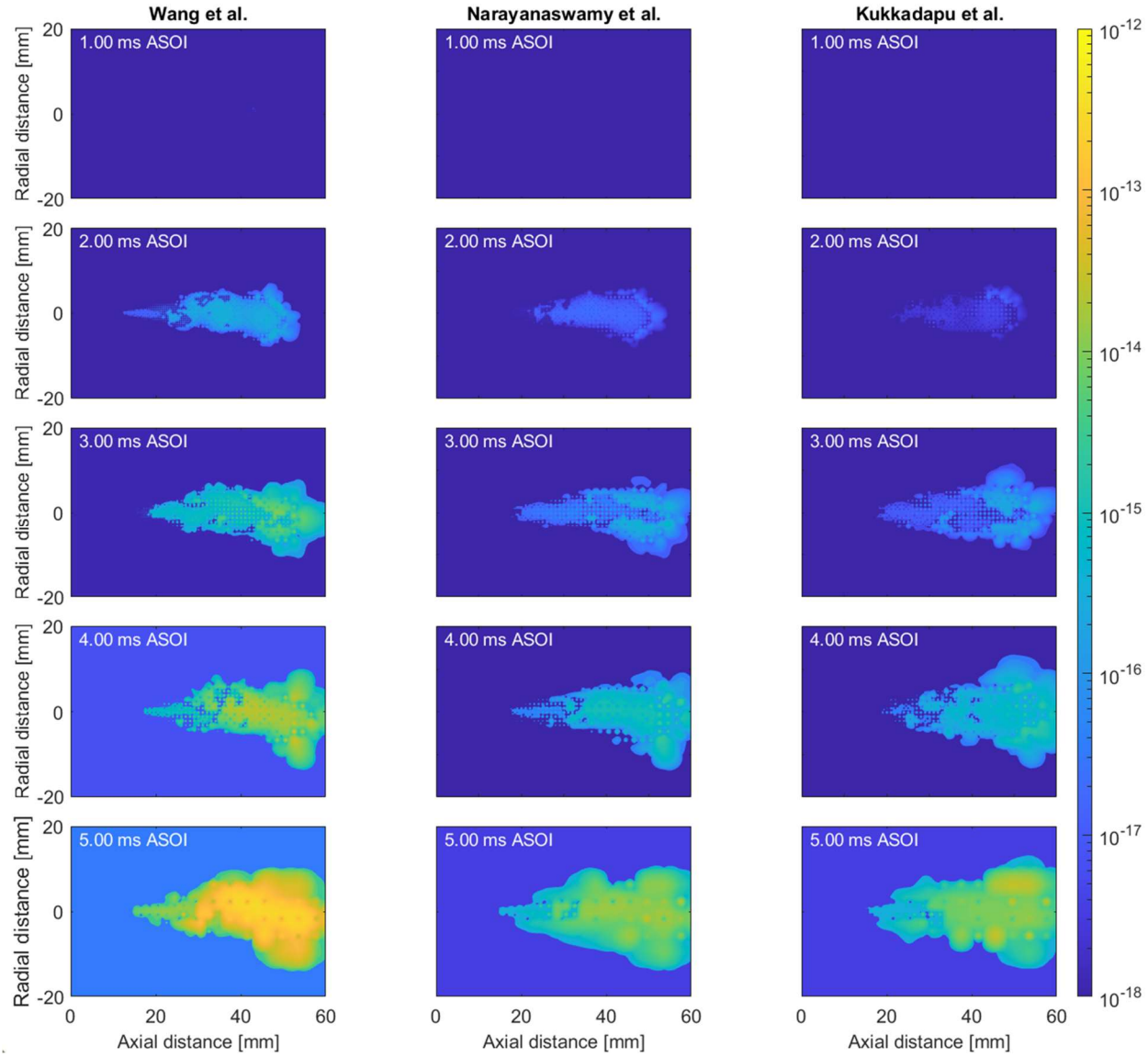

Figure 1. Projections of soot mass [kg-m] at select timings after the start of injection for simulations using the three mechanisms with the PSM soot model.

Figure 3 shows the cumulative soot mass predicted by different soot sub-models: inception, surface growth, fragmentation, oxidation, condensation, and coagulation for two of the chemical mechanisms: Wang et al. [17] and Kukkadapu et al. [19]. While the total soot mass predicted is similar between the PSM and PM models, their respective sub-models behave differently. In both models, the inception process is a major contributor to soot mass. The PSM model predicts a higher rate of inception than the PM model for both mechanisms by at least an order of magnitude. The PM model shows almost no contribution to total soot mass from the inception process after about 5 ms. This is expected due to the model's two-way coupling implementation that leads to the depletion of the pyrene soot precursor, as shown in Figure 2a. While inception drives soot mass increase in the early stage, condensation eventually dominates soot formation.

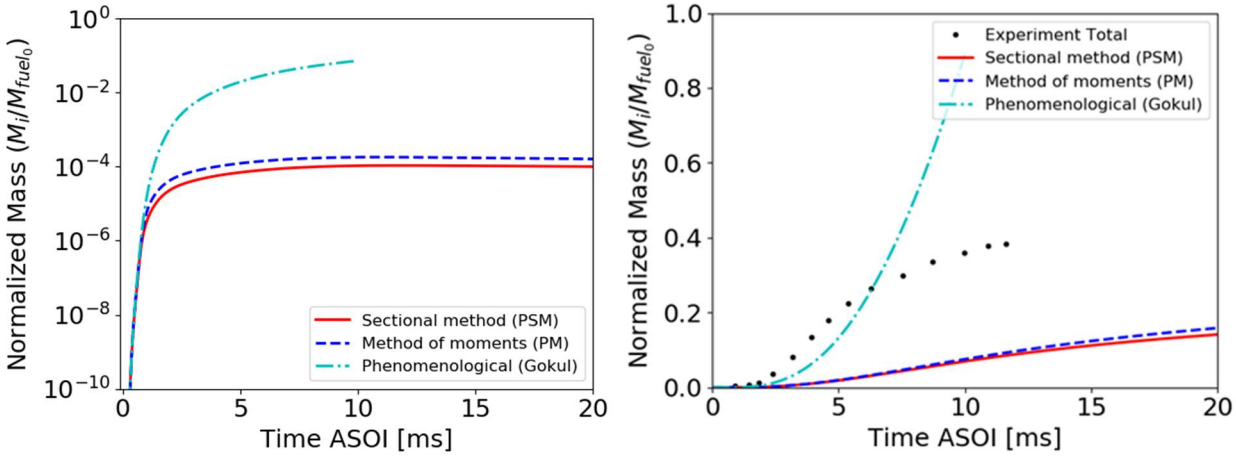

Figure 2: a) Time-resolved profiles of the mass of pyrene normalized by the mass of injected n-dodecane and b) total soot mass profiles normalized by the mass of injected n-dodecane predicted by different soot models with the Wang et al. *[17]* mechanism. Experimentally measured total soot mass are obtained from *[4]*.

For both the Wang et al. and the Kukkadapu et al. mechanisms, soot mass from condensation is higher for the PM model compared to the PSM model. There are also differences in the surface growth, but the condensation term is a couple orders of magnitude higher. This indicates that smaller gas phase species such as C_2H_2 react primarily with other gas phase species rather than soot particles. These gas phase reactions are driven by the chemical mechanisms whereas surface growth is modeled via the Hydrogen Abstraction Acetylene Addition Ring Closure (HACARC) mechanism [20] within the soot model. The HACARC mechanism mimics the reaction of smaller gas phase species with solid soot particles. Due to the oxygen deficient nature of the charge gas, soot oxidation is not a significant process. While the PM model shows a small amount of soot oxidation, it is still at least two orders of magnitude below other soot related phenomena.

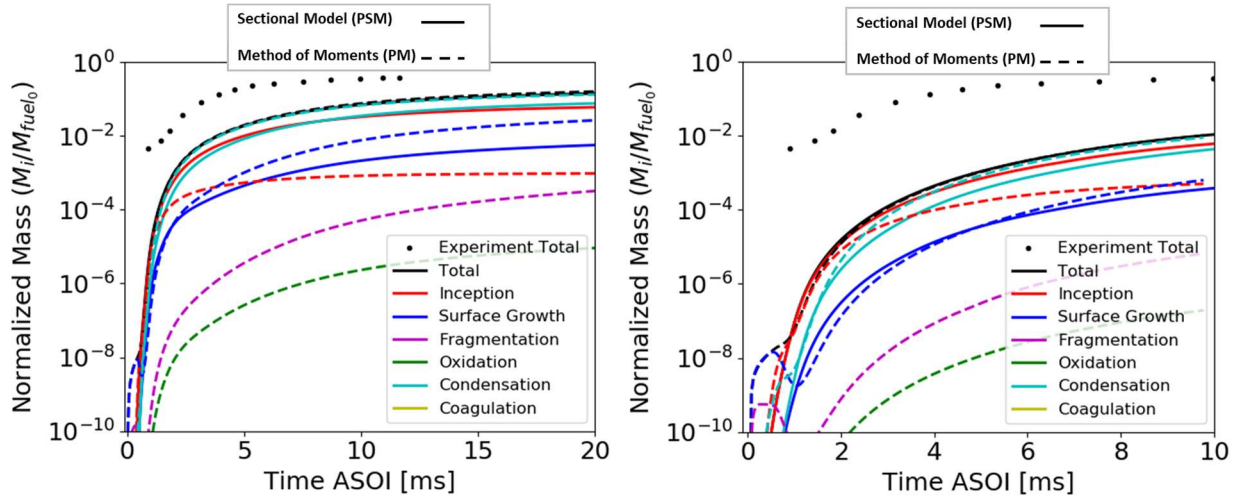

Figure 3: Cumulative soot mass normalized by mass of injected n-dodecane versus time ASOI with contributions from different sub-models for the PSM and PM soot models with two kinetic mechanisms: a) Wang et al. [17] and b) the Kukkadapu et al [19].

We compare the effect of the three different chemical mechanisms when using the PSM soot model in Figure 3, which shows the cumulative soot mass predicted by different soot sub-models. As anticipated based on Figure 1, the Wang et al. mechanism results in higher soot mass than the other two mechanisms with substantial differences in the early stages, and still about an order of magnitude gap by 20 ms between the Wang et al. (highest) and Narayanaswami et al. (lowest). Inception and condensation drive soot growth, as previously discussed, with the contributions from the two terms being of the same order. There is a time delay between inception and condensation since inception is the primary soot growth mechanism in the initial period. The Wang et al. mechanism shows a cross-over around 8 ms, with condensation becoming the dominating contributor, but the other two mechanisms show nearly matched contributions for these two processes by the end of the simulation time. Surface growth is the next largest term, but several orders of magnitude smaller and does not make a large contribution to the total soot mass.

Inception is predicted to occur at a higher rate initially for the Narayanaswamy et al. mechanism than for the Kukkadapu et al. counterpart. This is primarily due to the precursor that was used for each as can be seen in Table 2 (A_3R5, A_4, fluoranthene, and A_4R5 for the Narayanaswamy et al., only A_4R5 for the Kukkadapu et al.). As seen in Figure 1, the simulations with the Narayanaswamy et al. mechanism predict more soot in the early stages. However, the Kukkadapu et al. mechanism predicts higher soot mass after about 3 ms. The contribution of both inception and condensation processes surpass those predicted using the Narayanaswamy et al. mechanism at these later times. It is also worth noting that surface growth contributes more to the increase in soot mass with the Wang et al. mechanism compared to the other two mechanisms.

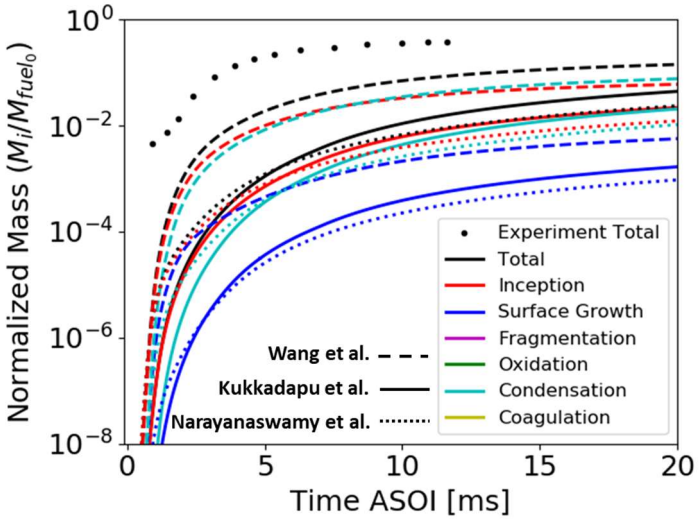

Figure 4: Cumulative soot mass normalized by mass of injected n-dodecane versus time ASOI with contributions from different sub-models for the PSM soot model with the Kukkadapu et al. *[19]* Narayanaswamy et al. *[18]*, and Wang et al. *[17]* mechanisms.

Some of the differences described above are due to the variations in gas phase species predicted by the chemical mechanisms and how they interact with the soot models. To study this effect, Figure 5 shows the mass of various species normalized by the mass of injected n-dodecane for the three different mechanisms shown in Table 2 with the PSM soot model. We can see that the

n-dodecane fuel breaks down more quickly for the two more detailed chemical mechanisms. These mechanisms contain a larger number of pathways to more accurately capture the fuel breakdown process. More C_2H_2 is formed initially by the Wang et al. compared to the other two mechanisms, which likely spurs the greater initial increase in soot mass. However, the Kukkadapu et al. mechanism predicts a higher formation rate of C_2H_2 compared to the Wang et al. mechanism beyond 7 ms, leading to the higher soot mass increase driven by surface growth observed in Figure 4. Note the Y-axis uses a log scale which can make small changes in the mass appear large for smaller absolute values such as the fuel as it is consumed at later times.

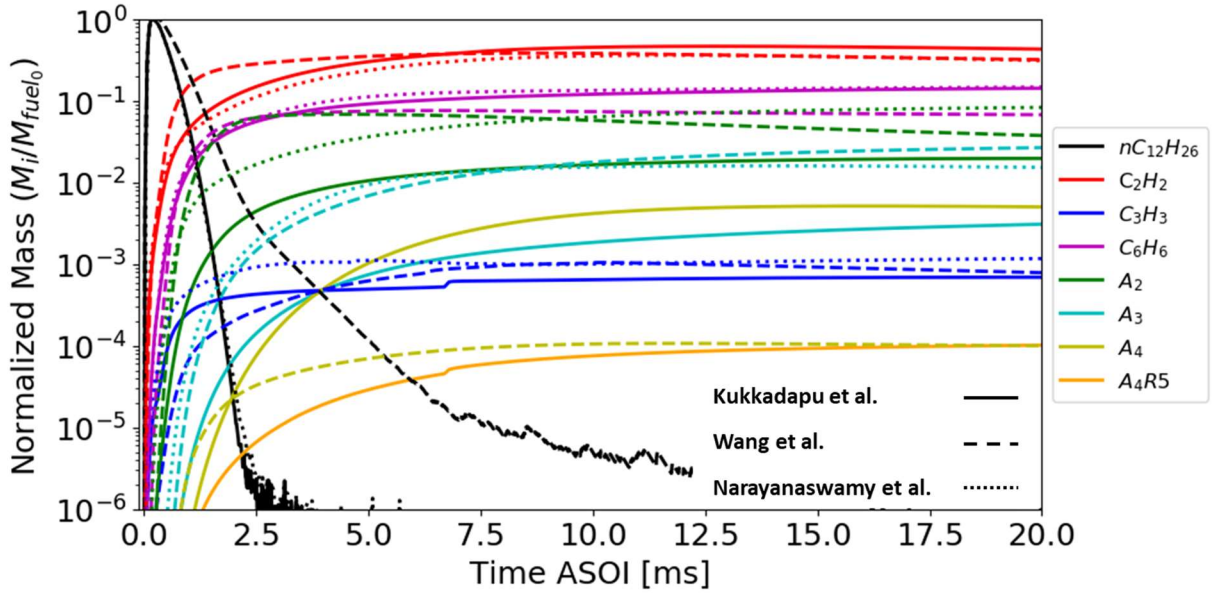

Figure 5: The mass for a number of species normalized by mass of injected n-dodecane for simulations with the Kukkadapu et al. *[19]*, Wang et al. *[17]* and Narayanaswamy et al. *[18]* mechanisms with the PSM soot model versus time ASOI.

Pyrene (A_4) is used as a precursor for simulations using the Wang et al. and Narayanaswamy et al. mechanisms along with other precursors for the Narayanaswamy et al. mechanism (see Table 2). Pyrene mass is below the range displayed in this plot for the Narayanaswamy et al. mechanism, expectedly because of rapid conversion to soot. In contrast, there is a higher amount of pyrene predicted by the Wang et al. mechanism, remaining at a near constant level until the end of the simulations. This indicates the formation rate of pyrene predicted by the gas phase kinetic mechanism is greater than its consumption rate within the PSM soot model throughout the simulation. The Kukkadapu et al. mechanism uses A_4R5 as the soot precursor, so direct comparison is difficult. The simulations results show that A_4R5 forms later than pyrene, which provides a sound explanation regarding the delay in soot formation for this mechanism compared to the other two, as seen in Figure 4. Other key species such as naphthalene (A_2) or anthracene (A_3) present substantial differences amongst the different mechanisms. This is likely the result of different pathways available in the kinetic mechanisms, with more detailed mechanisms generally leading to more reliable species concentrations. The present results show the simpler Wang et al. mechanism producing soot mass in better agreement with experiments than the other two kinetic mechanisms, which seems to contradict the previous sentence. To better understand this contradiction, future work will investigate fundamentals of species concentration for the different mechanisms, as well as, the role of PAH precursors in the soot formation process.

4. Conclusions

3-D CFD simulations of soot formation via fuel pyrolysis were carried out with finite rate chemistry using three detailed chemical kinetics models and three soot models available in CONVERGE. The simulation results were compared to experimental measurements to provide a frame of reference about the soot mass predicted by the different kinetic mechanisms and soot models. Oxygen-deficient, pyrolysis conditions serve as a good benchmark by removing the complexities associated with the competing processes driving soot formation and oxidation. All simulation results predict lower soot mass compared to the experiments, as well as later soot inception/formation. An important finding is that soot inception time depends on the species chosen as precursor(s), which link the chemical kinetics to the soot model. Choosing larger PAH molecules can lead to a delay in the prediction of soot onset compared to a smaller molecule. The simulations showed that the soot inception, condensation, and surface growth processes are highly dependent on the chemical mechanism. The formation of soot was somewhat uniform across the jet, which is in agreement with the experiments used as the target. This homogeneity indicates that mixing does not play a major role under these conditions, and support that a detailed turbulence model may not be needed to accurately capture the physics of soot formation. Therefore, a simplified approach such as the use of 0-D reactors can be employed to perform larger parametric variations with detailed kinetic mechanisms and advanced soot models in a computationally-efficient manner.

5. Acknowledgements

The authors would like to thank Convergent Sciences Inc. for licenses. This work was conducted as part of the Partnership for Advanced Combustion Engine (PACE) project sponsored by the U.S. Department of Energy (DOE) Office of Energy Efficiency and Renewable Energy (EERE), Bioenergy Technologies and Vehicle Technologies Offices. Lawrence Livermore National Laboratory is operated by Lawrence Livermore National Security, LLC, for the U.S. Department of Energy, National Nuclear Security Administration under Contract DE-AC52-07NA27344. Sandia National Laboratories is a multi-mission laboratory managed and operated by National Technology and Engineering Solutions of Sandia, LLC., a wholly owned subsidiary of Honeywell International, Inc., for the U.S. Department of Energy's National Nuclear Security Administration under contract DE-NA0003525.

6. References

[1] R. Newell, D. Raimi and G. Aldana, "Global Energy Outlook 2019: The Next Generation of Energy," Resources for the Future, 2019.

[2] "International Sooting Flame (ISF) workshop," 2021. [Online].

[3] K. J. Richards, P. K. Senecal and E. Pomraning, "CONVERGE (v3.0), Convergent Science," Madison, WI, 2020.

[4] S. A. Skeen and K. Yasutomi, "Measuring the soot onset temperature in high-pressure n-dodecane spray pyrolysis," *Combustion and Flame,* vol. 188, pp. 483-487, 2018.

[5] B. Launder and B. Sharma, "Application of the energy-dissipation model of turbulence to the calculation of flow near a spinning disc," *Letters in Heat and Mass Transfer,* vol. 1, no. 2, pp. 131-137, 1974.

[6] R. D. Reitz, "Modeling atomization processes in high-pressure vaporizing sprays," *Atomisation Spray Technology,* vol. 3, p. 309, 1987.

[7] P. K. Senecal, K. J. Richards, E. Pomraning, T. Yang, M. Z. Dai, R. M. McDavid, M. A. Patterson, S. Hou and T. Shethaji, "A New Parallel Cut-Cell Cartesian CFD Code for Rapid Grid Generation Applied to In-Cylinder Diesel Engine Simulations," in *SAE World Congress & Exhibition*, 2007.

[8] D. P. Schmidt and C. J. Rutland, "A new droplet collision algorithm," *Journal of Computational Physics,* vol. 164, no. 1, pp. 62-80, 2000.

[9] T. M. Nguyen, R. N. Dahms, L. M. Pickett and F. Tagliante, "The Corrected Distortion Model for Lagrangian Spray Simulation of Transcritical Fuel Injection," *In Preparation.*

[10] A. Babajimopoulos, D. N. Assanis, D. L. Flowers, S. M. Aceves and R. P. Hessel, "A fully coupled computational fluid dynamics and multi-zone model with detailed chemical kinetics for the simulation of premixed charge compression ignition engines," *International Journal of Engine Research,* vol. 6, no. 5, pp. 497-512, 2005.

[11] M. Frenklach and A. M. Mebel, "On the mechanism of soot nucleation.," *Physical Chemistry Chemical Physics,* vol. 22, no. 9, pp. 5314-5331, 2020.

[12] M. J. McNenly, R. A. Whitesides and D. L. Flowers, "Faster solvers for large kinetic mechanisms using adaptive preconditioners," *Proceedings of the Combustion Institute,* vol. 35, no. 1, pp. 581-587, 2015.

[13] J. Manin, M. Bardi, L. M. Pickett and R. Payri, "Boundary condition and fuel composition effects on injection processes of high-pressure sprays at the microscopic level.," *International Journal of Multiphase Flow,* vol. 83, pp. 267-278, 2016.

[14] J. Manin, L. Pickett and K. Yasutomi, "Stereoscopic high-speed microscopy to understand transient internal flow processes in high-pressure nozzles," *Experimental Thermal and Fluid Science,* vol. 114, p. 110027, 2020.

[15] M. P. B. Musculus and K. Kattke, "Entrainment Waves in Diesel Jets," *SAE International journal of engines,* vol. 2, no. 1, pp. 1170-1193, 2009.

[16] L. M. Pickett, J. Manin, C. L. Genzale, D. L. Siebers, M. P. B. Musculus and C. A. Idicheria, "Relationship Between Diesel Fuel Spray Vapor Penetration/Dispersion and Local Fuel Mixture Fraction," *SAE International journal of engines,* vol. 4, no. 1, pp. 764-799, 2011.

[17] H. Wang, Y. Ra, M. Jia and R. D. Reitz, "Development of a reduced n-dodecane-PAH mechanism and its application for n-dodecane soot predictions," *Fuel,* vol. 136, pp. 25-36, 2014.

[18] K. Narayanaswamy, P. Pepiot and H. Pitsch, "A chemical mechanism for low to high temperature oxidation of n-dodecane as a component of transportation fuel surrogates," *Combustion and Flame,* vol. 161, no. 4, pp. 866-884, 2014.

[19] G. Vishwanathan and R. Reitz, "Development of a Practical Soot Modeling Approach and its Application to Low Temperature Diesel Combustion," *Combustion Science and Technology,* vol. 182, no. 8, pp. 1050-1082, 2010.

[20] F. Mauss, "Entwicklung eines Kinetischen Modells der Russbildung mit Schneller," RWTH Aachen, Aachen, 1998.

[21] J. Z. Wen, M. J. S. H. Park, S. N. Rogak and M. F. Lightstone, "Study of Sooth Growth in a Plug Flow Reactor using a Moving Sectional Model," *Proceedings of the Combustion Institute ,* vol. 30, no. 1, pp. 1477-1484, 2005.

[22] S. Kumas and D. Ramkrishna, "On the Solution of Population Balance Equations by Discretization—II. A Moving Pivot Technique," *Chemical Engineering Science ,* vol. 51, no. 8, pp. 1333-1342, 1996.